Analysis of coronavirus temperature-sensitive mutants reveals an interplay between the macrodomain and papain-like protease impacting replication and pathogenesis

Xufang Deng[1], Robert C. Mettelman[1], Amornrat O'Brien[1], John A. Thompson[1], Timothy E. O'Brien[2], and Susan C. Baker[1,a]

[1]Department of Microbiology and Immunology, Loyola University Chicago, Stritch School of Medicine, Maywood, IL 60153

[2]Department of Mathematics and Statistics, Loyola University Chicago, Chicago, IL 60660

[a]Corresponding author:
Susan C. Baker, PhD
sbaker1@luc.edu

Running title: CoV macrodomain and PLP2 interplay impacts replication

Abstract

Analysis of temperature-sensitive (ts) mutant viruses is a classic method allowing researchers to identify genetic loci involved in viral replication and pathogenesis. Here, we report genetic analysis of a ts strain of mouse hepatitis virus (MHV), tsNC11, focusing on the role of mutations in the macrodomain and the papain-like protease 2 (PLP2) domain of nonstructural protein 3, a component of the viral replication complex. Using MHV reverse genetics, we generated a series of mutant viruses to define the contribution of macrodomain- and PLP2-specific mutations to the ts phenotype. Viral replication kinetics and efficiency of plating analysis performed at permissive and non-permissive temperatures revealed that changes in the macrodomain alone were both necessary and sufficient for the ts phenotype. Interestingly, mutations in the PLP2 domain were not responsible for the temperature sensitivity but did reduce the frequency of reversion of macrodomain mutants. Co-immunoprecipitation studies are consistent with an interaction between the macrodomain and PLP2. Expression studies of the macrodomain-PLP2 portion of nsp3 indicate that the ts mutations enhance the proteasome-mediated degradation of the protein. Furthermore, we found that during virus infection, the replicase proteins containing the MAC and PLP2 mutations were more rapidly degraded at the non-permissive temperature, as compared to the wild-type proteins. Importantly, we show that the macrodomain- and PLP2-mutant viruses trigger production of type I interferon *in vitro* and are attenuated in mice, further highlighting the importance of the macrodomain-PLP2 interplay in viral pathogenesis.

Importance

Coronaviruses are emerging human and veterinary pathogens with pandemic potential. Despite the established and predicted threat these viruses pose to human health, there are currently no approved countermeasures to control these infections in humans. Viral macrodomains, enzymes that remove post-translational ADP-ribosylation of proteins, and viral multifunctional papain-like proteases, enzymes that cleave polyproteins and remove polyubiquitin chains via deubiquitinating (DUB) activity, are two important virulence factors. Here, we reveal an unanticipated interplay between the macrodomain and the PLP2 domain that is important for replication and antagonizing the host innate immune response. Targeting the interaction of these enzymes may provide new therapeutic opportunities to treat CoV disease.

Introduction

Coronaviruses (CoVs) are enveloped, positive-sense, single-stranded RNA viruses that primarily infect the respiratory or gastrointestinal tract. CoVs can emerge from an animal reservoir, such as bats, to infect a new species and cause epidemic or pandemic disease with high mortality. Recent emergence events exemplified by Severe Acute Respiratory Syndrome coronavirus (SARS-CoV) and Middle East Respiratory Syndrome coronavirus (MERS-CoV) in humans (1), and Swine Acute Diarrhea Syndrome coronavirus (SADS-CoV) in domestic pigs (2), have demonstrated how devastating these viruses can be within naïve populations. To date, there are no approved antivirals or effective vaccines that protect humans from coronavirus

63 diseases. Therefore, identifying viral factors that contribute to pathogenesis and
64 characterizing novel targets for therapeutic interventions are two important approaches
65 to facilitate the development of effect vaccines and antivirals.

66 The murine coronavirus, mouse hepatitis virus (MHV), is widely used as a model
67 system to study coronavirus replication and pathogenesis in mice. The replication of the
68 virus initiates with the engagement of the spike glycoprotein with a host cell receptor
69 and the release of the positive-sense RNA into the cytoplasm of the cell. The large (~32
70 Kb) viral genomic RNA is translated to produce two long polyproteins, pp1a and pp1ab,
71 which are processed by viral proteases, including the papain-like proteases (PLP1
72 and/or PLP2), and the 3C-like protease (3CLpro or Mpro), into 16 nonstructural proteins
73 (nsp1-16, Figure 1A). To generate the viral replication complex, the coronaviral nsps
74 sequester host endoplasmic reticulum (ER) to generate convoluted membranes and
75 double-membrane vesicles (DMVs), which are the sites of viral RNA synthesis (3, 4).
76 The viral replication complex generates a nested-set of dsRNA intermediates to
77 produce copious amounts of mRNAs, which are then translated to produce the
78 structural (spike, envelope, membrane and nucleocapsid) and virus-specific accessory
79 proteins. The genomic RNA and structural proteins assemble in the ER-Golgi
80 intermediate compartment to generate infectious virus particles that are released from
81 the cell (5, 6).

82 CoV replication induces profound rearrangement of the host ER, and generates
83 viral dsRNA intermediates, processes that can be sensed by the host to activate the
84 innate immune response. As a result, CoVs have evolved multiple strategies to
85 counteract and delay activation of these host immune responses and establish an

environment amenable to virus replication. These strategies include: expressing species-specific accessory proteins as modulators of innate immune responses [reviewed in (7)]; encoding highly-conserved nonstructural proteins that serve as interferon antagonists (8–10) and sequestering viral RNA in DMVs (3, 4) to prevent detection by host pattern recognition receptors. A key component in the assembly of the DMVs is nsp3 (11, 12). To date, eleven distinct nsp3 domains have been identified using either bioinformatic approaches or enzymatic studies (Figure 1A). Here, we focus on two multifunctional components encoded within nsp3, the macrodomain and the papain-like protease 2.

The region researchers now term the macrodomain was originally identified in the 1990s as a highly-conserved domain of unknown function, termed the X domain, contained within the replicase polyprotein of rubella virus, hepatitis E virus (HEV) and coronaviruses (13–15). Structural and biochemical studies revealed that the X domain exhibited structural similarity to the cellular histone MacroH2a and catalyzed measurable ADP-ribose-1''-phosphatase (ADRP) activity (16–18), although the functional significance of this enzymatic activity was unclear. Using reverse genetics to inactivate the catalytic site of the enzyme, researchers found that ADRP activity was not essential for CoV replication in cultured cells (19). However, further studies revealed that an ADRP-catalytic mutant virus was attenuated in mice (20), and that ADRP activity in SARS-CoV and human CoV-229E mediated resistance to antiviral interferon responses (21). These findings were consistent with an essential role for enzymatic activity *in vivo*; although, the target for the ADRP activity was still unclear. A breakthrough came in 2016 from a study revealing that the macrodomain of hepatitis E

109 virus acts as an ADP-ribose hydrolase (22). ADP-ribosylation is a known post-
110 translational modification that regulates cellular activities (23); therefore, viral enzymes
111 that reverse this process could interrupt host-cell signaling. For CoVs, nsp3
112 macrodomain activity was shown to promote MHV-induced encephalitis (24) and
113 increase virulence during SARS-CoV infection (25).

114 Another highly-conserved enzyme contained within nsp3 is the papain-like
115 protease 2 (PLP2). For MHV, PLP2 is responsible for processing the nsp3/4 junction
116 using a highly-conserved LXGG/X cleavage site (26). Studies using SARS-CoV
117 revealed that the single papain-like protease encoded on nsp3 (termed PLpro) cleaves
118 all three sites at the amino-terminal end of the polyprotein (27). PLpro also functions as
119 a deubiquitinating enzyme (DUB), capable of removing polyubiquitin chains from
120 substrates (28, 29). Structural studies revealed that CoV PLpro/PLP2s are similar to
121 cellular DUBs (30). Enzymatic analysis revealed that CoV PLpro/PLP2s are
122 multifunctional with protease, deubiquitinating and deISGylating activity (30–33). The
123 viral DUB activity has been implicated as a modulator of the innate immune response to
124 viral infection (32, 34, 35), but the target(s) of the DUB activity have not yet been
125 identified. Thus, both the PLP2 and macrodomains of nsp3 have been independently
126 identified as contributors to coronavirus virulence.

127 In this study, we characterized a temperature-sensitive MHV mutant virus
128 containing mutations within both the macrodomain and PLP2 domain. We investigated
129 the contribution of these mutations to the temperature-sensitive phenotype as well as
130 the resulting effects on viral pathogenesis. The results presented here reveal a
131 previously undescribed interplay between the macrodomain and PLP2 domain that

impacts replication, antagonizes the innate immune response, and contributes to viral pathogenesis. Modulating the macrodomain-PLP2 interaction may provide new opportunities for therapeutic intervention.

Results

Identifying mutations associated with a temperature-sensitive phenotype. Murine coronavirus strain tsNC11 was generated by chemical mutagenesis, plaque purified, and validated as a temperature-sensitive (ts) mutant defective in positive-sense RNA synthesis at non-permissive temperatures (36). Complementation analysis indicated that tsNC11 harbored mutation(s) in the ORF1a region of the replicase polyprotein, but the specific mutations were unknown. To identify the nucleotide changes in tsNC11, we isolated the genomic RNA from viral supernatant, subjected it to deep sequencing then aligned the reads to the genomic sequence of MHV-A59 (GenBank accession #AY910861). In agreement with the complementation study by Schaad et al. (36), the sequence analysis revealed 7 non-synonymous substitutions in the ORF1a of tsNC11. These substitutions resulted in 7 amino acid changes: two in nsp2 (I4V and T543I), four in nsp3, and one in nsp10 (P23S). The four mutations within nsp3 are distributed between the macrodomain (K532E and G554D) and the PLP2 domain (D1026N and D1071N) (Figure 1A). As noted above, previous studies documented the importance of the macrodomain and PLP2 domain in virus replication and disease; therefore, we focused our efforts on evaluating how these substitutions contributed to the ts phenotype, the stability of the phenotype, and the pathogenesis of the virus in mice.

To evaluate the contributions of the macrodomain and PLP2 domain mutations to the ts phenotype, three mutant viruses were generated using the MHV-A59 reverse

155 genetics system (37). The first mutant virus, designated MACmut, contains the
156 macrodomain mutations K532E and G554D. The second virus was engineered with the
157 D1026N and D1071N mutations within the PLP2 domain and is designated PLP2mut.
158 The third virus, MAC/PLP2mut, combines the mutations in the macro- and PLP2
159 domains into one virus. In addition, an isogenic wild-type MHV (icWT) was used as a
160 control. These viruses were recovered, plaque purified, and propagated in DBT cells at
161 a permissive temperature of 32^{o}C. Deep-sequencing results confirmed the incorporation
162 of the desired nucleotide changes in nsp3 and revealed no additional amino acid
163 changes within the ORF1 region.

164 First, we evaluated the one-step growth curves of all 5 viruses (tsNC11, icWT
165 and the 3 engineered mutants) at the permissive (32^{o}C) and non-permissive (37^{o}C and
166 40^{o}C) temperatures. As expected, icWT replicates to high titer at all three temperatures,
167 whereas tsNC11 is impaired at both 37^{o}C and 40^{o}C, as reported by Schaad et al. (36)
168 (Fig. 1B). Analysis of the three engineered mutants revealed that the two substitutions
169 in the PLP2 domain were not sufficient to confer a temperature-sensitive phenotype, as
170 the kinetics of replication mirrored those of the wild-type virus. In contrast, the MACmut
171 virus exhibited reduced virus replication at 40^{o}C, but was only slightly impaired at 37^{o}C.
172 The MAC/PLP2 mutant virus mirrored the kinetics of tsNC11 with impaired replication at
173 both 37^{o}C and 40^{o}C, implicating the mutations in both the macro- and PLP2 domains as
174 contributors to the temperature-sensitive phenotype of tsNC11.

175 We also evaluated the plaque size and efficiency of plating (EOP) of the viruses
176 at permissive and non-permissive temperatures. As expected, all viruses replicated to
177 high titer and formed similarly-sized plaques at 32^{o}C (Figure 2, upper panel). tsNC11 is

178 profoundly temperature-sensitive, with a low number of plaques detected at the 10^{-1}
179 dilution plate incubated at the non-permissive temperature. The tsNC11 plaques that
180 were detected at the non-permissive temperature exhibited a large-plaque phenotype
181 suggesting that these viruses may be revertants. We found that the PLP2mut virus
182 formed large plaques at 40^{o}C, which is consistent with the results of the kinetic analysis
183 and indicates that the mutations in the PLP2 domain are not sufficient to cause the ts
184 phenotype. Analysis of the MACmut virus revealed a mixed population of small and
185 large plaques at the non-permissive temperature, the majority of which displayed the
186 small-plaque phenotype. The MAC/PLP2 mutant virus mirrored the plaque size and
187 plating efficiency of tsNC11. We calculated the EOP values, which represent the ratio of
188 viral titers obtained at 40^{o}C and 32^{o}C (Figure 2B). Again, both the PLP2mut and icWT
189 viruses had similar titers at both temperatures, resulting in an EOP of ~1. In contrast,
190 the MACmut virus exhibited titers that were significantly lower at 40^{o}C compared to
191 titers obtained at 32^{o}C (EOP=10^{-2}). These results indicate that the MACmut virus, but
192 not the PLP2mut or icWT viruses, has a defect in plaque formation at the non-
193 permissive temperature. Taken together, these data demonstrate that the mutations in
194 the macrodomain, but not those in the PLP2 domain, are the major determinants of the
195 ts phenotype of tsNC11. Additionally, these results are consistent with a critical role of
196 the macrodomain in viral replication. Interestingly, we found that the MAC/PLP2 mutant
197 virus mirrored the plaque size and low reversion frequency of tsNC11 (EOP = 10^{-5}),
198 supporting a role for the PLP2 domain as a genetic enhancer of the ts phenotype. A
199 genetic enhancer, as defined by genetic studies of eukaryotic organisms, is a mutation
200 in one gene that intensifies the phenotype caused by a mutation in another gene (38).

Evaluating revertants of the MACmut virus. While generating the MACmut virus, we noticed that, in addition to the majority population having the small-plaque phenotype, a subpopulation of large plaques were also present at 40^{o}C. The large plaques consistently appeared even after several rounds of plaque purification of the small-plaque isolates. Therefore, we asked if the small plaques were formed by temperature-sensitive viruses, while the large plaques were due to revertant viruses. To address this question, we selectively isolated plaques with different sizes and propagated them at 32^{o}C to obtain viral stocks for subsequent analysis (Figure 3). We found that the small-plaque isolates recapitulated the phenotype of the parental MACmut virus: small plaques and similar EOP values (Figure 3A). In contrast, the large-plaque isolates exhibited a phenotype similar to icWT. Sequencing results of PCR amplicons, representing the region spanning the macro- and PLP2 domains, revealed that small-plaque isolates had no additional mutations in either the macrodomain or PLP2. In contrast, the large-plaque isolates had either a true reversion (D554-to-G), or harbored putative suppressive mutations located within the macrodomain, or the adjacent, downstream sequence (Figure 3B). Among seven large-plaque revertants, all maintained the K532E mutation, indicating it was not associated with the ts phenotype. Three isolates had the D554-to-G reversion, suggesting that it may be sufficient for the ts phenotype of the MACmut virus. We found that isolates 4-7 maintained the engineered mutations, but had also acquired additional, potentially suppressive, mutations in the downstream region. Together, these results indicate that altering the coding sequence of either the macrodomain or the downstream region is likely sufficient to revert or suppress the ts phenotype caused by the G554D mutation. We also

224 evaluated the MAC-PLP2 region of tsNC11 large-plaque revertant viruses and found
225 that all three isolates had the D554-to-G reversion (Figure 3C), consistent with our
226 findings with the MACmut revertants.

227 **Mutations in PLP2 enhance the ts phenotype by reducing reversion frequency.**
228 We determined that the macrodomain mutations are the major contributors to the ts
229 phenotype; however, we noticed that the MACmut virus did not completely phenocopy
230 tsNC11. We found that the replication of the MACmut virus was defective at 40^{o}C, but
231 not at 37^{o}C. In addition, the MACmut virus exhibited a higher EOP value (10^{-2})
232 compared to that of tsNC11 (10^{-4}) (Fig 2B), indicating a relatively high reversion
233 frequency. These data imply that mutations *outside* the macrodomain may enhance the
234 ts phenotype by stabilizing the replication defect, thereby preventing reversion to the
235 wild-type phenotype (38). Therefore, we asked if the addition of the PLP2 mutations
236 observed in tsNC11 could enhance the ts phenotype of the MACmut virus and reduce
237 reversion. We found that the MAC/PLP2mut virus exhibits a severe replication defect at
238 both 37^{o}C and 40^{o}C (Figure 1B), and only replicated under permissive conditions,
239 similar to tsNC11. The MAC/PLP2mut and tsNC11 viruses exhibited similar EOP values
240 (~10^{-4}) (Figure 2B). Of note, the low titer of the MAC/PLP2mut virus at 40^{o}C indicates a
241 low level of reversion to the wild-type phenotype, suggesting that the PLP2 mutations
242 stabilize the MACmut virus. Taken together, these data demonstrate that while the
243 PLP2 mutations are not sufficient to cause the ts phenotype, they act to enhance the ts
244 phenotype caused by the mutation in the macrodomain. Enhancing phenotypes have
245 been described for other coronavirus interacting proteins (39, 40), which motivated us to

246 determine if the enhancement phenotype we detected here is due to an interaction
247 between the macro and PLP2 domains.

248 **Evaluating macrodomain interaction with the PLP2 domain.** The structures of
249 several domains of nsp3 have been solved individually [reviewed in (41)] or in
250 combination (42). However, owing to the size and complexity this protein, the complete
251 structure of nsp3 remains unsolved. The capacity of the PLP2 mutations to enhance the
252 ts phenotype in the presence of the macrodomain mutations raises the possibility of
253 domain-domain interaction between the macrodomain and PLP2. To test this
254 hypothesis, we generated plasmids that express either an epitope-tagged macrodomain
255 (HA-MAC) or PLP2 domain (PLP2-V5) (depicted in Figure 4A). When these plasmids
256 were co-transfected into HEK-293T cells, the expression of both the macrodomain and
257 PLP2 were detectable by the cognate epitope antibodies (Figure 4B). We detected HA-
258 MAC in lysates immunoprecipitated with anti-V5, and inversely, PLP2-V5 was detected
259 when HA-MAC was immunoprecipitated from the lysates. These results indicate that the
260 ectopically expressed macrodomain associates with PLP2 in cell lysates, consistent
261 with either a direct or indirect interaction.

262 **Mutations in the macrodomain and PLP2 domain affect protein stability.** Because
263 we found that mutation in the macrodomain (G554D) is the major ts determinant and the
264 PLP2 mutations enhance the ts phenotype, we reasoned that these mutations might
265 alter protein folding, thereby rendering the protein unstable and susceptible to
266 proteasome-mediated degradation. To determine if the mutations in the macrodomain
267 and/or the PLP2 domain alter protein stability, plasmid DNA expressing wild-type or
268 mutant forms of MAC/PLP2 polypeptide (Figure 5A) were transfected into HEK-293T

cells. The cells were maintained at 37^{o}C throughout the experiment. We added cycloheximide (CHX) at 16 hours post-transfection to block translation, and harvested cell lysates at the indicated times. The level of expressed proteins was determined by immunoblotting (Figure 5B and C). The MAC/PLP2 (WT) protein was maintained at levels comparable to those prior to treatment, up to 5 hours post-treatment with CHX. In contrast, we detected rapid reductions in the levels of all of the mutant forms of the protein. Addition of the proteasome inhibitor MG132 blocked the degradation of the proteins (Figures 5B and 5C). These results indicate that mutations in both the MAC and PLP2 domains affect the protein folding and stability, rendering the proteins more susceptible to proteasome-mediated degradation.

To determine if these MAC/PLP2 mutations affect the stability of the replicase proteins during virus replication at the non-permissive temperature, we performed temperature shift experiments as outlined in Figure 6. We infected cells with either WT or MAC/PLP2mut virus and incubated at the permissive temperature for 9.5 h. At this point, we added CHX to block translation and shifted the infected-cells to the non-permissive temperature. Cell lysates were collected every 30 minutes and evaluated using immunoblotting for the level of nonstructural intermediate nsp2-3 and product nsp3. We found that WT nsp2-3 and nsp3 were relatively stable, with loss of detection occurring at 3 hours after the temperature shift and addition of CHX (Fig 6C, lanes 2-8). In contrast, the levels of nsp2-3 and nsp3 in the MAC/PLP2mut-infected cells diminished more rapidly, with reduced levels at 1.5 hours after the temperature shift and addition of CHX (Fig 6C, lanes 9-15). These results support the finding that the MAC

and PLP2 mutations destabilize the replicase protein at the non-permissive temperature.

ts mutant viruses induce interferon in macrophages and are attenuated in mice. Previous studies have shown that the papain-like protease domains of MHV, SARS-CoV, and MERS-CoV antagonize the IFN response, likely through the deubiquitinating activity of these enzymes (32, 34, 35, 43–46). In addition, coronaviral macrodomains have been shown to suppress IFN production both *in vitro* and *in vivo* (20, 21, 24, 25). We asked if the mutations in the macrodomain and PLP2 modulate the type I IFN response during infection of macrophages. As shown in Figure 7A, infection of mouse bone marrow-derived macrophages (BMDMs) with mutant viruses at permissive temperature produced significantly more IFN-α during infection compared to the icWT virus infection. At 12 hours post-infection, the MACmut virus induced 2-fold more IFN-α than icWT virus. Furthermore, the level of N gene transcript, which reveals the abundances of all viral mRNAs, was reduced in the MACmut-infected cells, compared to the wild type virus. We found that the PLP2mut virus elicited dramatically more IFN-α than WT virus, while the level of N gene expression was similar. The MAC/PLP2mut virus exhibited the most robust IFN-α and the lowest level of N gene expression. These results show that mutations in the macrodomain and the PLP2 domain result in elevated levels of type I IFN mRNA expression during infection of macrophages, further supporting the role of macrodomain and PLP2 in modulating host innate immunity.

Because the ts mutant viruses had reduced replication efficiency and elicited type I IFN production during infection of macrophages, we were interested in evaluating the pathogenicity of these viruses. To this end, C57BL/6 mice were intracranially

inoculated with 600 plaque-forming units (PFUs) of virus and monitored for weight loss and mortality. As shown in Figure 7B, all WT virus-infected mice lost weight rapidly and succumbed to infection by day 11 post-infection. In contrast, the mutant virus-infected mice exhibited transient or no weight loss during the infection period and all mice survived. These results demonstrate that the ts mutant viruses are attenuated *in vivo*, and those mutations adjacent to the catalytic sites of the macro- and PLP2 domains can modulate viral pathogenesis.

Discussion

Identifying viral factors that modulate the immune response to viral infection provides new opportunities for developing novel antiviral interventions. Here, we described an unanticipated interplay between two previously characterized virulence factors, the macrodomain and the papain-like protease, of coronaviruses. The enzymatic activities of these domains have been implicated in removing post-translational modifications: macrodomains remove mono- or poly-ADP-ribose from proteins (18, 22, 23); deubiquitinating activity of viral papain-like proteases removes mono- or poly-ubiquitin chains from signaling proteins (30, 32, 47). Our study stems from characterizing a temperature-sensitive mutant virus that harbored mutations within both the macrodomain and the PLP2 domain of nsp3. We found that the mutation within the macrodomain (G554D) was associated with the most significant temperature-sensitive phenotype, but that this alteration of the macrodomain reverted to the wild-type phenotype at high frequency. However, viruses containing mutations in both the macrodomain and PLP2 domain reverted less frequently, consistent with the PLP2

337 domain having an enhancing effect on the ts phenotype. Although these two enzymes
338 reside within the same nsp3 polypeptide (Figure 1A), to our knowledge, this is the first
339 suggestion of an interplay between these domains. By expressing the macrodomain
340 and papain-like protease 2 domain on independent expression plasmids, we were able
341 to evaluate and detect co-immunoprecipitation of the proteins, consistent with either a
342 direct or indirect interaction. Furthermore, we report that the mutations identified in the
343 macrodomain and PLP2 domain destabilize the proteins, as revealed by proteasome-
344 dependent degradation. Lastly, we demonstrate that these mutant viruses promote type
345 I IFN production from macrophages in tissue culture and are attenuated in mice. This
346 work confirms and extends previous studies that independently identified the
347 macrodomain and the papain-like protease 2 domain as modulators of the innate
348 immune response and virulence factors [reviewed in (31, 48, 49), (35)].

349 Macrodomains have been shown to play a role in the virulence of positive-sense
350 RNA viruses including hepatitis E virus (HEV), alphaviruses, and coronaviruses
351 [reviewed in (48, 49)]. Studies of the alphavirus Chikungunya virus (CHIKV) revealed
352 that the macrodomain at the N terminus of nsP3 hydrolyzes ADP-ribose groups from
353 mono-ribosylated proteins and that this de-ribosylating activity is critical for CHIKV
354 replication in vertebrate and insect cells, and for virulence in mice (50). Interestingly,
355 viruses engineered to encode a mutation of the CHIKV macrodomain catalytic site
356 rapidly reverted to the wild-type sequence (51), similar to the high frequency reversion
357 we reported for the MHV MACmut virus (Figure 3). Studies of the role of the
358 macrodomain during coronavirus replication indicate that catalytic activity is not required
359 for virus replication in interferon non-responsive cell lines (19, 20, 24). However,

360 catalytic activity is important for replication in primary cells and in mice, implicating the
361 macrodomain in evading the innate immune response and promoting viral pathogenesis
362 (20, 24, 25). Identifying the ribosylated substrates that are targeted by the viral
363 enzymatic activity is an important future direction for this work.

364 Our study implicated an adjacent viral domain, the papain-like protein 2 domain,
365 as an interacting partner with the macrodomain. Interestingly, the helicase domain
366 adjacent to the macrodomain of hepatitis E virus (HEV) was found to modulate
367 macrodomain activity. Biochemical assays revealed that the presence of the HEV
368 helicase domain *in cis* enhanced the binding of the macrodomain to ADP-ribose and
369 stimulated the hydrolase activity (22). Furthermore, we previously found that the
370 mutations in the Ubl-2 domain could cause a ts phenotype and destabilize the PLP2
371 domain (52). Here, we found that the mutations in the macro- and PLP2 domains
372 destabilized the replicase proteins, as shown by the more rapid degradation of the
373 proteins after temperature shift. We speculate that there may be a dynamic interaction
374 between adjacent domains within the nsp3 polyproteins.

375 As a multidomain protein, nsp3 must hold a sophisticated architecture to function
376 properly and precisely. To date, four essential functions have been documented for this
377 multidomain protein: 1) interaction of the Ubl-1 domain with the nucleocapsid (N) protein
378 is important for genomic RNA synthesis and encapsidation (39, 40); 2) proteolytic
379 processing of the N-terminal region of pp1a and pp1ab to release nsp1, nsp2, and nsp3
380 (26, 27); 3) hijacking the cellular reticular network in concert with other membrane-
381 associated proteins (nsp4 and nsp6) to form virus-specific membrane structures for
382 RNA synthesis (11, 12); and 4) antagonizing the innate immune response through the

383 actions of the de-ADP-ribosylating activity of the macrodomain and the deubiquitinating
384 activity of the PLP2 domain [reviewed in (31, 48)]. The removal of post-translational
385 modifications such as ADP-ribosylation and poly-ubiquitination could be directed either
386 at cellular proteins to redirect them for use during viral replication, or to subvert
387 signaling of innate immune responses. Ultimately, structural and biochemical studies
388 will be needed to fully investigate the multiple *cis* and *trans* interactions of nsp3 and to
389 determine if there is a dynamic interplay that modulates the stability, substrate
390 specificity and/or affinity of the enzymes and substrates.

391 We found that the MAC/PLP2mut virus recapitulated the ts phenotype of tsNC11
392 (Figure 1B). However, it is possible that some or all of the other mutations we identified
393 by deep sequencing (I4V and T543I in nsp2 and P23S in nsp10) may contribute in a
394 subtle way to the phenotype of tsNC11. Nsp2 was shown to be dispensable for MHV
395 and SARS-CoV replication, but the deletion of the nsp2 coding sequence resulted in
396 decreased viral replication and RNA synthesis (53). For nsp10, previous studies
397 revealed that this protein plays critical roles in the 3C-like protease-mediated
398 polyprotein processing and viral RNA synthesis (54, 55). The results from these studies
399 indicate that the mutations in nsp2 and nsp10 may also contribute to a ts phenotype.
400 While our study focuses on the contribution of the macrodomain and PLP2, further
401 studies are needed to fully evaluate the impact of other ORF1a mutations on the
402 replication and pathogenesis of coronaviruses.

403 In summary, we report what is, to our knowledge, the first indication of an
404 interplay between the macrodomain and papain-like protease 2 domain of CoV nsp3.
405 We found that this interplay impacts virus replication efficiency, innate immune

antagonism and virulence in mice. A detailed understanding of the relationship between the macro- and PLP2 domains will require further structural and enzymatic studies. We anticipate that the genetic analysis, co-immunoprecipitation and *in vivo* pathogenesis outcomes reported here will facilitate these future studies.

Materials and Methods

Virus and cells. Human embryonic kidney (HEK) 293T cells (CRL-11268, ATCC) were cultured in Dulbecco's modified Eagle medium (DMEM) with 10% fetal bovine serum (FBS) and 2% L-glutamine. Delayed brain tumor (DBT) cells were grown in minimal essential media (MEM) (catalog no. 21800-0400; Gibco) supplemented with 10% tryptose phosphate broth (TPB) media, 5% heat-inactivated FBS (Atlanta Biological), 2% penicillin/streptomycin (pen/strep; HyClone), and 2% L-glutamine. The BHK-MHVR cell line was kindly provided by Mark Denison at Vanderbilt University Medical Center and cultured in Dulbecco's modified Eagle medium (DMEM) (catalog no. 12100-046, Gibco) supplemented with 10% heat-inactivated FBS and G418 (0.8 mg/mL; HyClone). Differentiated BMDMs were maintained in bone marrow macrophage media containing DMEM (catalog no. 10-017-CV, Corning) supplemented with 30% L929 cell supernatant, 20% FBS, 1% L-glutamine, 1% sodium pyruvate, and 1% pen/strep. HeLa-MHVR cells (56) were grown in DMEM (catalog no. 12100-046, Gibco) supplemented with 10% FBS, 1% L-glutamine, 0.5% HEPES, and 1% pen/strep. Temperature-sensitive MHV strain tsNC11 was propagated in DBT cells at 32˚C. The infectious clone MHV-A59 strain (GenBank accession no. AY910861) serves as wild-type (icWT) virus for this study.

Deep sequencing and bioinformatic analysis. Viral RNA was extracted from the supernatant of tsNC11-infected DBT cells incubated at 32˚C. Isolated RNA was sent to GENEWIZ, Inc. for cDNA library preparation and Illumina Miseq high-throughput sequencing. Raw reads were subject to pairing and trimming and aligned to the genome sequence of the synthetic construct of MHV A59 strain (GenBank accession no. AY910861) using Geneious software (Geneious R7, https://www.geneious.com). A medium-low sensitivity and an iteration of up to 5 times were chosen. A total of 195,824 sequences with a mean coverage of 898.8 were aligned to the MHV Synthetic Construct template. Polymorphisms were detected using the "find variations/SNPs" tool. Parameters included a minimum coverage of 5 with a minimum variant frequency of 25% in order for a variation to be called. The maximum variant p-value was set at 10^{-6} and the minimum strand bias p-value was set at 10^{-5} when exceeding 65% bias. We focused our analysis on the first 12 kb of the replicase gene, since previous studies reported the ts phenotype was associated with changes in this region (36, 57).

Generation of mutant viruses. All infectious clones were generated using the reverse genetics system previously established for MHV-A59 (37). Mutations identified by deep sequencing within the macrodomain and PLP2 domain were introduced into plasmids A and B, respectively, then verified by sequencing of the plasmid DNA. DNA fragments were ligated together and used for *in vitro* transcription of viral RNA. *In vitro* transcribed genomic RNA and N gene RNA was electroporated into BHK-MHVR cells, which were overlaid onto DBT cells in a T75 flask. These cells were incubated at the permissive temperature of 32^{o}C to facilitate the replication of ts mutant viruses. Supernatants were collected at the time when cytopathic effect was evident, usually between 36 and 48 h

post-electroporation. All infectious clone mutant viruses were plaque purified, propagated on DBT cells, and subjected to full genome sequencing to validate the genotype. These infectious clones were designated MACmut, PLP2mut, and MAC/PLP2, according the locations of introduced mutations as shown in Figure 1.

Temperature-sensitive assay and one-step growth kinetics. To determine the temperature sensitivity of mutant viruses, the efficiency of plating (EOP = titer 40^{o}C/ titer 32^{o}C) of virus was measured. DBT cells were seeded into two 6-well plates at 5.0 x 10^5 cells/well a day prior to infection. Each viral stock supernatant was serially diluted and inoculated onto the DBT cells. After 1 h incubation at 37^{o}C, inoculum was removed, and cells were subsequently overlaid with 0.8% 2x MEM/agar mixture. One plate was incubated at 32^{o}C for 60 h, and the second plate was incubated at 40^{o}C for 48 h. Agarose-covered cells were fixed using 4% formaldehyde for 1 h and stained using 0.1% crystal violet solution after removal of agarose. Plaques were counted and titers were calculated.

To evaluate the kinetics of virus replication, a one-step growth curve was generated at each temperature. Briefly, DBT cells were infected with the designated virus at multiplicity of infection of 5 for 1 h at 37^{o}C, then plates were incubated at the specified temperatures. The supernatants were collected at indicated time points and titrated on DBT cells incubated at 32^{o}C for 60 h.

Isolation and characterizations of ts revertants. To isolate ts revertants, plaque assays were performed at 40^{o}C. Viruses from single plaques were isolated and propagated in DBT cells at 32^{o}C to obtain viral stocks. To determine the ts phenotype of the isolates, the isolates were titrated at both 32^{o}C and 40^{o}C and the EOP values were

475 calculated as described above. To identify any mutations within the region of macro-
476 and PLP2 domains of the revertants, viral genomic RNA was extracted using
477 TriReagent (MRC, Inc.) according to the manufacturer's instruction and subsequently
478 subject to cDNA synthesis. A genomic region (3976-6101 nt) containing the macro- and
479 PLP2 domain was amplified by PCR using specific primers (Sense: 5'- CAA GAA AGG
480 TCT TTA GGG CTG CTT -3'; anti-sense: 5'- GAC ACC ATC AAC CTT CTC AAA TG -
481 3'). The PCR products were sequenced and the sequencing results were compared to
482 the tsNC11 sequence.

483 **MAC and PLP2 expression plasmids.** Nucleotide sequences encoding the
484 macrodomain [467-622 amino acids (aa) of nsp3] were amplified from a codon-
485 optimized MHV nsp3 gene (sequence available upon request) and cloned into pCAGGS
486 vector with an HA epitope tag, designated as HA-MAC. The pCAGGS-PLP2 plasmid
487 (PLP2-V5) was generated in a previous study (52). The coding sequence of the
488 macrodomain through PLP2 domain (467-1085 aa) was inserted into pcDNA3.1 and
489 fused with a c-terminal V5 epitope tag (pMP-WT). Mutations were introduced into these
490 constructs using site-directed mutagenesis PCR or Gibson Assembly technique to
491 generate pMP-GD (G554D), pMP-2DN (D1026N/D1071N) and pMP-GD/2DN
492 (G554D/D1026N/D1071N), which all contain a c-terminal V5 tag.

493 **Co-immunoprecipitation.** HA-MAC and PLP2-V5 plasmids were co-transfected into
494 HEK-293T cells in 35 mm dishes. Cells were harvested using 500 μL lysis buffer (20
495 mM Tris pH 7.5, 150 mM NaCl, 1 mM EGTA, 1 mM EDTA, 1% Triton X-100, 2.5 mM
496 sodium pyrophosphate, 1 mM β-glycerophosphate, 1 mM sodium ortho-vanadate, 1
497 μg/mL leupeptin, 1 mM PSMF) and 200 μg of whole cell lysates were used for

498 immunoprecipitation with 1 μg primary mouse anti-V5 (R96025, Invitrogen) or -HA
499 (MMS-101R-200, Biolegend) monoclonal antibody (Ab). Protein-Ab mixtures were
500 rotated at 4°C overnight and then added 15 μL magnetic protein G beads
501 (LSKMAGA02, Millipore) for 1 h incubation. Beads were washed three times with
502 washing buffer (lysis buffer composition except 450 mM NaCl) and eluted with 40 μL 2x
503 sample buffer (10% glycerol, 5% β-ME, 3% SDS, 7.5 mg/mL Trizma-base, bromophenol
504 blue). Eluted products and 5% of cell lysates as input were subject to SDS-PAGE gel
505 electrophoresis and immune-blotting with anti-V5 or anti-HA antibodies.

506 **Evaluating protein stability after addition of cycloheximide.** To determine the
507 steady-state level of protein, 0.5 μg of the specified plasmid DNA was transfected into
508 HEK-293T cells with transfection reagent TransIT-LT1 (MIR2300, Mirus) according to
509 the manufacture's recommendation. At 16 h post-transfection, cells were treated with 20
510 μg/mL of cycloheximide (CHX) (5087390001, Sigma Aldrich) or a combination of 20
511 μg/mL CHX and 10 μM MG132 (474790, Calbiochem), a proteasome inhibitor, and
512 harvested at the indicated time points. Equal amounts of cell lysate were subjected to
513 immunoblotting with anti-V5 or anti-β-actin (A00702, Genscript) antibodies. The relative
514 intensity of MAC/PLP2 bands (relative to β-actin) were measured and calculated with
515 AlphaView software (Protein Simple). To assess the rate of decay of the protein amount
516 over time for the four viral protein types, we fit the two-parameter simple exponential
517 nonlinear regression function, $y = \theta_1 e^{-\theta_2 x}$, using the NLIN procedure in SAS 9.4
518 software package and verified using Minitab software version 18. In this regression
519 equation, θ_1 is the initial viral amount parameter at time zero and θ_2 is the slope or rate

of decay parameter. The slope parameters (θ_2) were each compared with the WT slope using NLIN's provided two-sided t-tests and p-values < 0.05 were deemed significant.

To evaluate the steady level of replicase proteins nsp2-3 and nsp3, we performed a temperature shift experiment. Briefly, HeLa-MHVR cells were infected with either WT or MAC/PLP2mut virus (moi = 5) and incubated at the permissive temperature for 9.5 h, when the cells were shifted to 40^{o}C and treated with 20 ug/mL of CHX. Whole cell lysates were prepared at 30 min intervals by the addition of lysis buffer A (4% SDS, 3% DTT, 40 % glycerol and 0.065 M Tris, pH 6.8). The lysates were passed through a 25-gage needle to break up aggregates, incubated at 37^{o}C for 30 min and loaded onto a 6% SDS-PAGE, followed by transfer to a nylon membrane. The membrane was incubated with a 1:2,000 dilution of rabbit polyclonal anti-nsp2-3 antibody (anti-D3) (58), followed by horseradish peroxidase (HRP)-conjugated donkey anti-rabbit IgG (H+L) (Southernbiotech), and developed with Western Lightening Plus-ECL reagents (PerkinElmer). The membrane was stripped and re-probed using a 1:2,000 dilution of mouse anti-calnexin antibody, followed by HRP-conjugated goat anti-mouse IgG (H+L), and developed as above.

Reverse transcription quantitative PCR (RT-qPCR). The protocol of RT-qPCR was described previously (9) with slight modification. Briefly, BMDMs were mock-infected or infected with wild-type or mutant MHVs at a multiplicity of infection (MOI) of 1 and incubated at a permissive temperature of 32 ^{o}C. At indicated time points, cells were harvested for RNA extraction using an RNeasy Mini Kit (74104, Qiagen). An equal amount of RNA was used for cDNA synthesis using Rt2 HT First Strand Kit (330401, Qiagen). To determine IFN-α11, β-actin, or MHV-A59 N gene mRNA production, qPCR

was performed with specific primers for mouse IFN-α11 (PPM03050B-200, Qiagen), mouse β-actin (PPM02945B-200, Qiagen) or MHV-A59 N gene (Sense: 5'- AGC AGA CTG CAA CTA CTC AAC CCA ACT C -3'; anti-sense: 5'- GCA ATA GGC ACT CCT TGT CCT TCT GCA -3') using RT2 SYBR Green qPCR Mastermix (330502, Qiagen) in the Bio-Rad CFX96 system. The thermocycler was set as follows: one step at 95 °C (10 min), 40 cycles of 95 °C (15 s), 60 °C (1 min) and plate read, one step at 95 °C (10 s), and a melt curve from 65 °C to 95 °C at increments of 0.5 °C/0.05 s. Samples were evaluated in triplicate and data are representative of three independent experiments. The levels of mRNA were relative to β-actin mRNA and expressed as $2^{-\Delta CT}$ [$\Delta CT = C_{T(\text{gene of interest})} - C_{T(\beta\text{-actin})}$].

Evaluating viral pathogenesis. The protocol for evaluating pathogenesis of MHV was approved by the Loyola University Chicago IACUC and previously described (59). Briefly, six-week-old C57BL/6 female mice were purchased from the Jackson Laboratory. Mice were intracranially inoculated with 600 PFU in 20 μL PBS and monitored daily for changes in body weight. Infected mice were euthanized when weight loss was over 25% according to the protocol. Statistical analysis of survival rate was evaluated using the log-rank test.

Acknowledgements

We thank Dr. Ralph S. Baric, The University of North Carolina at Chapel Hill, for providing tsNC11. We thank Dr. Catherine Putonti at Loyola University Chicago for advice on the bioinformatic analysis. This work was supported by the National Institutes of Health grant R01 AI085089 (to SCB). R.C.M. was supported by the (NIH) T32

Training Grant for Experimental Immunology (#AI007508) and the Arthur J. Schmitt Dissertation Fellowship in Leadership and Service (Arthur J. Schmitt Foundation).

Author contributions

X.D. and S.C.B. conceived the concept, planned the experiments, and wrote the manuscript with contributions from all authors. X.D., R.C.M., and A.O. performed specific experiments and analyzed the data. J.A.T performed the bioinformatic analysis. T.E.O. conducted the statistical analysis. Current contact information for J.A.T. is jtho46@lsuhsc.edu

References

1. de Wit E, van Doremalen N, Falzarano D, Munster VJ. 2016. SARS and MERS: Recent insights into emerging coronaviruses. Nat Rev Microbiol 14:523–534.

2. Zhou P, Fan H, Lan T, Yang X-L, Shi W-F, Zhang W, Zhu Y, Zhang Y-W, Xie Q-M, Mani S, Zheng X-S, Li B, Li J-MJ, Guo H, Pei G-Q, An X-P, Chen JJ-W, Zhou L, Mai K-J, Wu Z-X, Li D, Anderson DE, Zhang L-B, Li S-Y, Mi Z-Q, He T-T, Cong F, Guo P-J, Huang R, Luo Y, Liu X-L, Chen JJ-W, Huang Y, Sun Q, Zhang X-L-L, Wang Y-Y, Xing S-Z, Chen Y-S, Sun Y, Li J-MJ, Daszak P, Wang L-F, Shi Z-L, Tong Y-G, Ma J-Y. 2018. Fatal swine acute diarrhoea syndrome caused by an HKU2-related coronavirus of bat origin. Nature 556:255–258.

3. Gosert R, Kanjanahaluethai A, Egger D, Bienz K, Baker SC. 2002. RNA replication of mouse hepatitis virus takes place at double-membrane vesicles. J Virol 76:3697–3708.

4. Knoops K, Kikkert M, Worm SHE van den, Zevenhoven-Dobbe JC, van der Meer Y, Koster AJ, Mommaas AM, Snijder EJ. 2008. SARS-coronavirus replication is supported by a reticulovesicular network of modified endoplasmic reticulum. PLoS Biol 6:e226.

5. Enjuanes L, Almazán F, Sola I, Zuñiga S. 2006. Biochemical aspects of coronavirus replication and virus-host interaction. Annu Rev Microbiol 60:211–230.

6. Perlman S, Netland J. 2009. Coronaviruses post-SARS: update on replication and pathogenesis. Nat Rev Microbiol 7(6):439–50.

7. Kindler E, Thiel V, Weber F. 2016. Interaction of SARS and MERS Coronaviruses with the Antiviral Interferon Response, p. 219–243. *In* Advances in virus research.

8. Kindler E, Gil-Cruz C, Spanier J, Li Y, Wilhelm J, Rabouw HH, Züst R, Hwang M, V'kovski P, Stalder H, Marti S, Habjan M, Cervantes-Barragan L, Elliot R, Karl N, Gaughan C, van Kuppeveld FJM, Silverman RH, Keller M, Ludewig B, Bergmann CC, Ziebuhr J, Weiss SR, Kalinke U, Thiel V. 2017. Early endonuclease-mediated evasion of RNA sensing ensures efficient coronavirus replication. PLOS Pathog 13:e1006195.

9. Deng X, Hackbart M, Mettelman RC, O'Brien A, Mielech AM, Yi G, Kao CC, Baker SC. 2017. Coronavirus nonstructural protein 15 mediates evasion of dsRNA sensors and limits apoptosis in macrophages. Proc Natl Acad Sci U S A 114:E4251–E4260.

10. Menachery VD, Gralinski LE, Mitchell HD, Dinnon KH, Leist SR, Yount BL,

608 McAnarney ET, Graham RL, Waters KM, Baric RS. 2018. Combination
609 attenuation offers strategy for live-attenuated coronavirus vaccines. J Virol
610 92:e00710-18.

611 11. Oudshoorn D, Rijs K, Limpens RWAL, Groen K, Koster AJ, Snijder EJ, Kikkert M,
612 Bárcena M. 2017. Expression and cleavage of Middle East respiratory syndrome
613 coronavirus nsp3-4 polyprotein induce the formation of double-membrane
614 vesicles that mimic those associated with coronaviral RNA replication. MBio
615 8:e01658-17.

616 12. Neuman BW. 2016. Bioinformatics and functional analyses of coronavirus
617 nonstructural proteins involved in the formation of replicative organelles. Antiviral
618 Res 135:97–107.

619 13. Dominguez G, Wang C-Y, Frey TK. 1990. Sequence of the genome RNA of
620 rubella virus: Evidence for genetic rearrangement during togavirus evolution.
621 Virology 177:225–238.

622 14. Gorbalenya AE, Koonin E V., Lai MM-C. 1991. Putative papain-related thiol
623 proteases of positive-strand RNA viruses Identification of rubi- and aphthovirus
624 proteases and delineation of a novel conserved domain associated with proteases
625 of rubi-, α- and coronaviruses. FEBS Lett 288:201–205.

626 15. Koonin E V, Gorbalenya AE, Purdy MA, Rozanov MN, Reyes GR, Bradley DW.
627 1992. Computer-assisted assignment of functional domains in the nonstructural
628 polyprotein of hepatitis E virus: delineation of an additional group of positive-
629 strand RNA plant and animal viruses. Proc Natl Acad Sci U S A 89:8259–63.

630 16. Egloff M-P, Malet H, Putics A, Heinonen M, Dutartre H, Frangeul A, Gruez A,
631 Campanacci V, Cambillau C, Ziebuhr J, Ahola T, Canard B. 2006. Structural and
632 functional basis for ADP-ribose and poly(ADP-ribose) binding by viral macro
633 domains. J Virol 80:8493–502.

634 17. Saikatendu KS, Joseph JS, Subramanian V, Clayton T, Griffith M, Moy K,
635 Velasquez J, Neuman BW, Buchmeier MJ, Stevens RC, Kuhn P. 2005. Structural
636 basis of severe acute respiratory syndrome coronavirus ADP-Ribose-1″-
637 phosphate dephosphorylation by a conserved domain of nsP3. Structure
638 13:1665–1675.

639 18. Putics A, Gorbalenya AE, Ziebuhr J, Putics Á, Gorbalenya AE, Ziebuhr J. 2006.
640 Identification of protease and ADP-ribose 1″-monophosphatase activities
641 associated with transmissible gastroenteritis virus non-structural protein 3. J Gen
642 Virol 87:651–656.

643 19. Putics A, Filipowicz W, Hall J, Gorbalenya AE, Ziebuhr J. 2005. ADP-ribose-1"-
644 monophosphatase: a conserved coronavirus enzyme that is dispensable for viral
645 replication in tissue culture. J Virol 79:12721–31.

646 20. Eriksson KK, Cervantes-Barragán L, Ludewig B, Thiel V. 2008. Mouse hepatitis
647 virus liver pathology is dependent on ADP-ribose-1''-phosphatase, a viral function
648 conserved in the alpha-like supergroup. J Virol 82:12325–34.

649 21. Kuri T, Eriksson KK, Putics A, Züst R, Snijder EJ, Davidson AD, Siddell SG, Thiel
650 V, Ziebuhr J, Weber F. 2011. The ADP-ribose-1''-monophosphatase domains of
651 severe acute respiratory syndrome coronavirus and human coronavirus 229E

652 mediate resistance to antiviral interferon responses. J Gen Virol 92:1899–905.

653 22. Li C, Debing Y, Jankevicius G, Neyts J, Ahel I, Coutard B, Canard B. 2016. Viral
654 macro domains reverse protein ADP-ribosylation. J Virol 90:8478–86.

655 23. Jankevicius G, Hassler M, Golia B, Rybin V, Zacharias M, Timinszky G, Ladurner
656 AG. 2013. A family of macrodomain proteins reverses cellular mono-ADP-
657 ribosylation. Nat Struct Mol Biol 20:508–514.

658 24. Fehr AR, Athmer J, Channappanavar R, Phillips JM, Meyerholz DK, Perlman S.
659 2015. The nsp3 macrodomain promotes virulence in mice with coronavirus-
660 induced encephalitis. J Virol 89:1523–36.

661 25. Fehr AR, Channappanavar R, Jankevicius G, Fett C, Zhao J, Athmer J,
662 Meyerholz DK, Ahel I, Perlman S. 2016. The conserved coronavirus
663 macrodomain promotes virulence and suppresses the innate immune response
664 during severe acute respiratory syndrome coronavirus infection. MBio 7:e01721-
665 16.

666 26. Kanjanahaluethai A, Baker SC. 2000. Identification of mouse hepatitis virus
667 papain-like proteinase 2 activity. J Virol 74:7911–21.

668 27. Harcourt BH, Jukneliene D, Kanjanahaluethai A, Bechill J, Severson KM, Smith
669 CM, Rota PA, Baker SC. 2004. Identification of severe acute respiratory
670 syndrome coronavirus replicase products and characterization of papain-like
671 protease activity. J Virol 78(24):13600–12.

672 28. Barretto N, Jukneliene D, Ratia K, Chen Z, Mesecar AD, Baker SC. 2005. The

673 papain-like protease of severe acute respiratory syndrome coronavirus has
674 deubiquitinating activity. J Virol 79(24):15189–15198.

675 29. Lindner HA, Fotouhi-Ardakani N, Lytvyn V, Lachance P, Sulea T, Ménard R.
676 2005. The papain-like protease from the severe acute respiratory syndrome
677 coronavirus is a deubiquitinating enzyme. J Virol 79(24):15199–208.

678 30. Ratia K, Saikatendu KS, Santarsiero BD, Barretto N, Baker SC, Stevens RC,
679 Mesecar AD. 2006. Severe acute respiratory syndrome coronavirus papain-like
680 protease : Structure of a viral deubiquitinating enzyme. Proc Natl Acad Sci U S A
681 103(15):5717–22.

682 31. Mielech AM, Chen Y, Mesecar AD, Baker SC. 2014. Nidovirus papain-like
683 proteases: Multifunctional enzymes with protease, deubiquitinating and
684 deISGylating activities. Virus Res 194:184–190.

685 32. Bailey-Elkin BA, Knaap RCM, Johnson GG, Dalebout TJ, Ninaber DK, van
686 Kasteren PB, Bredenbeek PJ, Snijder EJ, Kikkert M, Mark BL. 2014. Crystal
687 structure of the MERS coronavirus papain-like protease bound to ubiquitin
688 facilitates targeted disruption of deubiquitinating activity to demonstrate its role in
689 innate immune suppression. J Biol Chem 289:34667–82.

690 33. Báez-Santos YM, Mielech AM, Deng X, Baker S, Mesecar AD. 2014. Catalytic
691 function and substrate specificity of the papain-like protease domain of nsp3 from
692 the Middle East respiratory syndrome coronavirus. J Virol 88:12511–27.

693 34. Devaraj SG, Wang N, Chen Z, Chen Z, Tseng M, Barretto N, Lin R, Peters CJ,
694 Tseng C-TK, Baker SC, Li K. 2007. Regulation of IRF-3-dependent innate

695 immunity by the papain-like protease domain of the severe acute respiratory
696 syndrome coronavirus. J Biol Chem 282(44):32208–21.

697 35. Niemeyer D, Mösbauer K, Klein EM, Sieberg A, Mettelman RC, Mielech AM,
698 Dijkman R, Baker SC, Drosten C, Müller MA. 2018. The papain-like protease
699 determines a virulence trait that varies among members of the SARS-coronavirus
700 species. PLOS Pathog 14:e1007296.

701 36. Schaad MC, Stohlman SA, Egbert J, Lum K, Fu K, Wei T, Baric RS. 1990.
702 Genetics of mouse hepatitis virus transcription: identification of cistrons which
703 may function in positive and negative strand RNA synthesis. Virology 177:634–45.

704 37. Yount B, Denison MR, Weiss SR, Ralph S, Baric RS. 2002. Systematic assembly
705 of a full-length infectious cDNA of mouse hepatitis virus strain A59. J Virol
706 76:11065–11078.

707 38. Herman RK, Yochem J. 2005. Genetic enhancers, p. 1–11. *In* WormBook.

708 39. Hurst KR, Ye R, Goebel SJ, Jayaraman P, Masters PS. 2010. An interaction
709 between the nucleocapsid protein and a component of the replicase-transcriptase
710 complex is crucial for the infectivity of coronavirus genomic RNA. J Virol
711 84:10276–10288.

712 40. Hurst KR, Koetzner CA, Masters PS. 2013. Characterization of a critical
713 interaction between the coronavirus nucleocapsid protein and nonstructural
714 protein 3 of the viral replicase-transcriptase complex. J Virol 87:9159–72.

715 41. Lei J, Kusov Y, Hilgenfeld R. 2018. Nsp3 of coronaviruses: Structures and

716 functions of a large multi-domain protein. Antiviral Res 149:58–74.

717 42. Chen Y, Savinov SN, Mielech AM, Cao T, Baker SC, Mesecar AD. 2015. X-ray
718 structural and functional studies of the three tandemly linked domains of non-
719 structural protein 3 (nsp3) from murine hepatitis virus reveal conserved functions.
720 J Biol Chem 290:25293–306.

721 43. Zheng D, Chen G, Guo B, Cheng G, Tang H. 2008. PLP2, a potent deubiquitinase
722 from murine hepatitis virus, strongly inhibits cellular type I interferon production.
723 Cell Res 18:1105–1113.

724 44. Yang X, Chen X, Bian G, Tu J, Xing Y, Wang Y, Chen Z. 2014. Proteolytic
725 processing, deubiquitinase and interferon antagonist activities of Middle East
726 respiratory syndrome coronavirus papain-like protease. J Gen Virol 95:614–626.

727 45. Mielech AM, Kilianski A, Baez-Santos YM, Mesecar AD, Baker SC. 2014. MERS-
728 CoV papain-like protease has deISGylating and deubiquitinating activities.
729 Virology 450–451:64–70.

730 46. Frieman M, Ratia K, Johnston RE, Mesecar AD, Baric RS. 2009. Severe acute
731 respiratory syndrome coronavirus papain-like protease ubiquitin-like domain and
732 catalytic domain regulate antagonism of IRF3 and NF-kappaB signaling. J Virol
733 83(13):6689–705.

734 47. Ratia K, Kilianski A, Baez-Santos YM, Baker SC, Mesecar A. 2014. Structural
735 basis for the ubiquitin-linkage specificity and deISGylating activity of SARS-CoV
736 papain-like protease. PLoS Pathog 10:e1004113.

737 48. Fehr AR, Jankevicius G, Ahel I, Perlman S. 2017. Viral macrodomains: unique
738 mediators of viral replication and pathogenesis. Trends Microbiol 26:598–610.

739 49. Leung AKL, McPherson RL, Griffin DE. 2018. Macrodomain ADP-ribosylhydrolase
740 and the pathogenesis of infectious diseases. PLOS Pathog 14:e1006864.

741 50. McPherson RL, Abraham R, Sreekumar E, Ong S-E, Cheng S-J, Baxter VK,
742 Kistemaker HA V., Filippov D V., Griffin DE, Leung AKL. 2017. ADP-
743 ribosylhydrolase activity of Chikungunya virus macrodomain is critical for virus
744 replication and virulence. Proc Natl Acad Sci 114:1666–1671.

745 51. Abraham R, Hauer D, McPherson RL, Utt A, Kirby IT, Cohen MS, Merits A, Leung
746 AKL, Griffin DE. 2018. ADP-ribosyl-binding and hydrolase activities of the
747 alphavirus nsP3 macrodomain are critical for initiation of virus replication. Proc
748 Natl Acad Sci U S A 115:E10457–E10466.

749 52. Mielech AM, Deng X, Chen Y, Kindler E, Wheeler DL, Mesecar AD, Thiel V,
750 Perlman S, Baker SC. 2015. Murine coronavirus ubiquitin-like domain is important
751 for papain-like protease stability and viral pathogenesis. J Virol 89:4907–4917.

752 53. Graham RL, Sims AC, Brockway SM, Baric RS, Denison MR. 2005. The nsp2
753 replicase proteins of murine hepatitis virus and severe acute respiratory syndrome
754 coronavirus are dispensable for viral replication. J Virol 79:13399–13411.

755 54. Donaldson EF, Sims AC, Graham RL, Denison MR, Baric RS. 2007. Murine
756 hepatitis virus replicase protein nsp10 is a critical regulator of viral RNA synthesis.
757 J Virol 81:6356–6368.

758 55. Donaldson EF, Graham RL, Sims AC, Denison MR, Baric RS. 2007. Analysis of
759 murine hepatitis virus strain A59 temperature-sensitive mutant TS-LA6 suggests
760 that nsp10 plays a critical role in polyprotein processing. J Virol 81:7086–7098.

761 56. Gallagher TM. 1996. Murine coronavirus membrane fusion is blocked by
762 modification of thiols buried within the spike protein. J Virol 70:4683–4690.

763 57. Baric RS, Fu K, Schaad MC, Stohlman SA. 1990. Establishing a genetic
764 recombination map for murine coronavirus strain A59 complementation groups.
765 Virology 177:646–656.

766 58. Schiller JJ, Kanjanahaluethai A, Baker SC. 1998. Processing of the coronavirus
767 MHV-JHM polymerase polyprotein: identification of precursors and proteolytic
768 products spanning 400 kilodaltons of ORF1a. Virology 242:288–302.

769 59. Deng X, StJohn SE, Osswald HL, O'Brien A, Banach BS, Sleeman K, Ghosh AK,
770 Mesecar AD, Baker SC. 2014. Coronaviruses resistant to a 3C-like protease
771 inhibitor are attenuated for replication and pathogenesis, revealing a low genetic
772 barrier but high fitness cost of resistance. J Virol 88:11886–11898.

773

774 **Figure legends**

775 **Figure 1. Evaluating the replication kinetics of coronavirus temperature-sensitive**
776 **mutants at permissive and non-permissive temperatures.** (A) Schematic diagram of
777 the MHV genome and the domains of nsp3. Abbreviations: Ubl1, ubiquitin-like domain 1;
778 Ac, acidic region; PLP1, papain-like protease 1; MAC, Macrodomain; DPUP, domain

779 proceeding Ubl2 and PLP2; Ubl2, ubiquitin-like domain 2; PLP2, papain-like protease 2;
780 NAB, nucleic acid-binding domain; G2M, coronavirus group 2 marker domain; TMDs,
781 transmembrane domains; Y, coronavirus highly-conserved domain. Representative
782 structures of the macrodomain with ribose (229E; PDB: 3EWR) and PLP2 (MHV; PDB:
783 4YPT) are shown in cyan and green with catalytic pockets circled and the residues
784 involved in catalysis shown in magenta. The mutations described in this study are
785 shown in red. (B) Growth kinetics of MHV and mutants at three temperatures. DBT cells
786 were inoculated with the indicated virus (MOI of 5) for 1 h at 37^{o}C and then shifted to
787 the indicated temperatures. Culture supernatant was collected at the indicated hours
788 post-infection and titrated in DBT cells at 32^{o}C. The data are representative of two
789 independent experiments. Error bars indicate ±SD.

790

791 **Figure 2. Analysis of plaque size and efficiency of plating at the permissive and**
792 **non-permissive temperatures.** (A) Representative plaque assays at 32^{o}C and 40^{o}C
793 for icWT, tsNC11 and engineered mutant viruses. The dilution of the viral stock is
794 indicated and selected to visualize ~20-50 plaques per plate. (B) Efficiency of plating
795 (EOP) = average titer at 40^{o}C/ average titer at 32^{o}C.

796

797 **Figure 3. Analysis of small- and large-plaque variants in the MACmut virus**
798 **population**. (A) MACmut isolates with distinct plaque sizes were evaluated for a ts
799 phenotype. Sequence analysis of individual plaque-purified revertant isolates identified

800 mutations in the macrodomain and the adjacent downstream region in the large-plaque
801 variants of the MACmut (B) and tsNC11(C) viruses.

802

803 **Figure 4. Evaluating co-immunoprecipitation of the macrodomain and the PLP2**
804 **domain.** (A) Schematic diagram of the individual constructs used to evaluate potential
805 interactions between the macrodomain and PLP2. (B) Western blotting to identify
806 expression and co-immunoprecipitation of HA-MAC and PLP2-V5. HEK-293T cells were
807 transfected with the indicated plasmid DNAs, lysates were prepared at 18 hours post-
808 transfection, subjected to immunoprecipitation with the indicated antibody and the
809 products analyzed by SDS-PAGE and immunoblotting. The data represent the results of
810 three independent experiments. Astersks indicate the cross detection of IgG chains by
811 secondary antibody.

812

813 **Figure 5. Mutations in macrodomain and PLP2 enhance degradation of the**
814 **polypeptide.** (A) Schematic diagram of constructs used to evaluate protein stability. (B
815 and C) Western blotting detecting wild-type or mutant forms of MAC-PLP2 polypeptide
816 in the presence of cycloheximide (CHX) or a combination of CHX and a proteasome
817 inhibitor MG132. HEK-293T cells were transfected with the indicated expression
818 plasmid of wild-type (WT) or mutant forms of MAC-PLP2. At 16 h post-transfection, cells
819 were treated with 20 μg/mL of CHX or a combination of 20 μg/mL CHX and 10 μM
820 MG132 and harvested at the indicated time points. Equal amount of cell lysate were
821 subjected to immunoblotting with anti-V5 or anti-β-actin antibodies. The relative intensity

of MAC/PLP2 bands (relative to β-actin) were measured and calculated with AlphaView software. The experiment was repeated two times and the representative immunoblots (B) and the curves of relative intensity (C) are shown. The slope parameters of the decay curves were evaluated using non-linear regression and two-sided t-tests compared to WT. **, P<0.005; ****, P<0.0001.

Figure 6. Mutations in the macrodomain and PLP2 alter the stability of replicase protein nsp3. HeLa-MHVR cells were infected with either icMHV-WT or MAC/PLP2mut virus (MOI of 5) and incubated at 32^{o}C for 9.5 h, then 20 μg/mL of cycloheximide (CHX) was added and cells were shifted to the non-permissive temperature. Lysates were prepared every 30 min, and the proteins separated by SDS-PAGE, and nonstructural proteins nsp2-3 and nsp3 were visualized by immunoblotting. A) Schematic diagram of MHV replicase polyprotein indicating the processing pathway and the region identified by the anti-nsp2-3 antibody. B) Outline of the experiment. C) Western blot evaluating the level of nsp2-3 and nsp3 proteins detected after shift to the non-permissive temperature. This is representative data of two independent experiments. Arrowhead indicates detections of cellular protein in all lysates. Asterisk indicates degradation products detected by anti-nsp2-3 antibody in the MAC/PLP2mut virus-infected cells.

Figure 7. Macrodomain mutant viruses induce type I interferon in primary macrophages and are attenuated in mice. (A) Mouse bone marrow-derived

macrophages were infected with the indicated virus (MOI of 1) at 32°C. Total RNA was extracted at the indicated time points and subjected to RT-qPCR. The mRNA levels of IFN-α (left) and N gene (right) are presented relative to β-actin. The results are representative of three independent experiments and subjected to a two-tailed, unpaired t-test. Error bars indicate ±SD. ***, P<0.001; ****, P<0.0001. n.s.: not significant. N.D.: not detected. (B) Six-week-old mice were injected intracranially with either icWT or the indicated ts mutant virus (600 PFU per mouse) and monitored for weight loss. Viral pathogenicity was evaluated by body weight loss (left) and percent survival (right). The number (n) of infected mice is indicated in parentheses. Error bars indicate ± SEM. Differences in survival rates were calculated using a log-rank test.

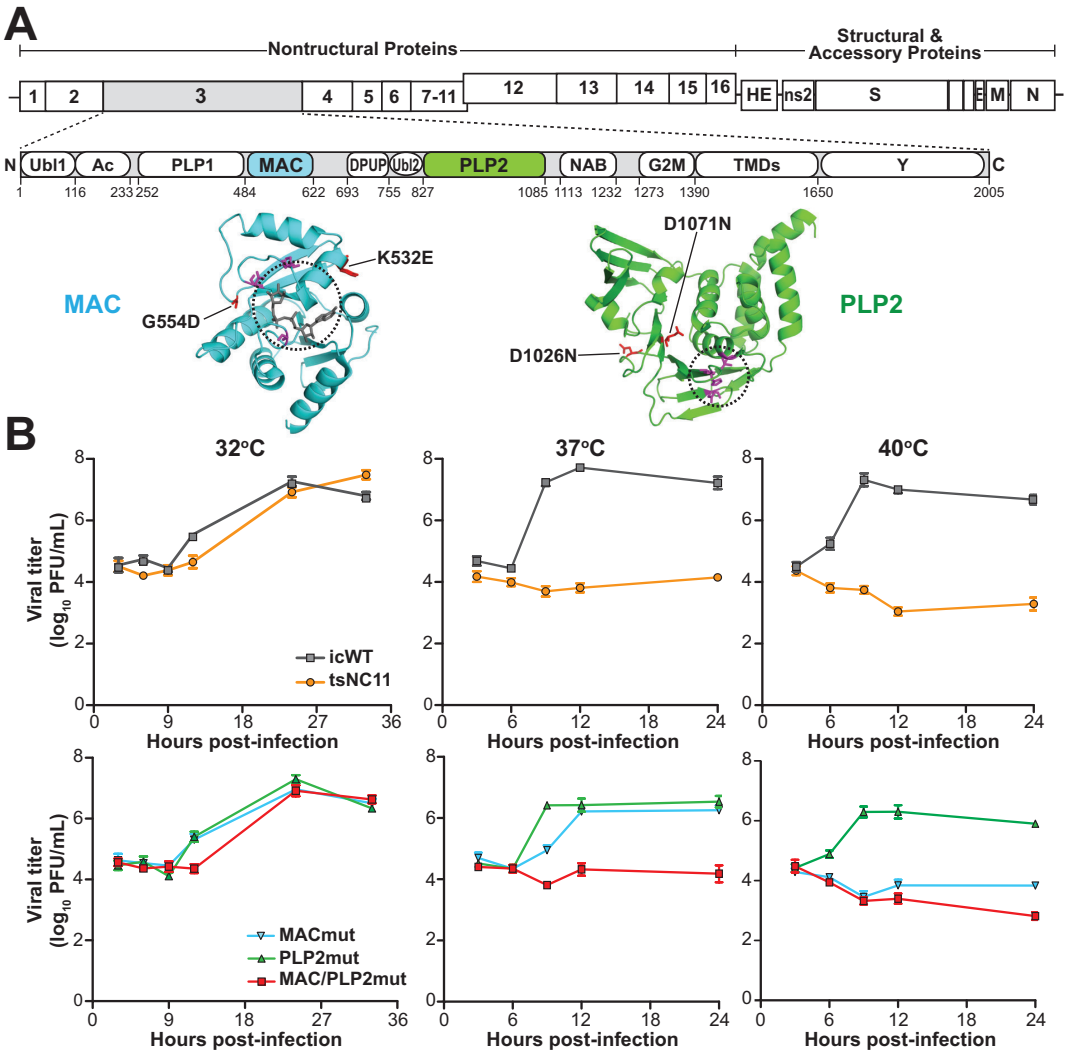

A

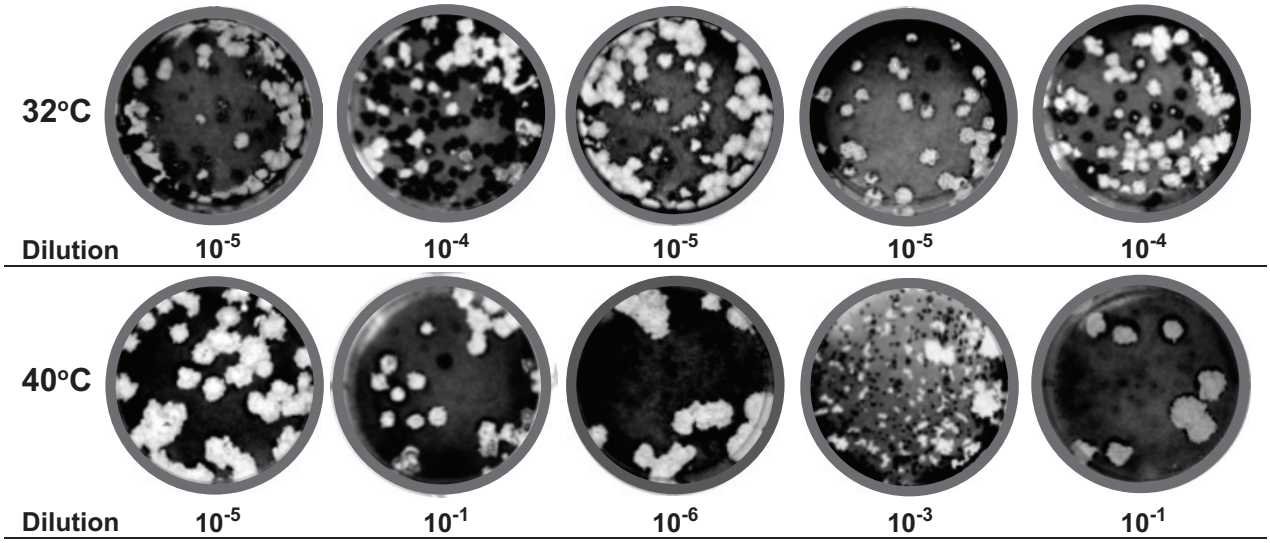

B

Virus Strain	Titer (PFU/mL) 32°C	Titer (PFU/mL) 40°C	EOP
icWT	2.0×10^{7}	1.3×10^{7}	0.7×10^{0}
tsNC11	4.0×10^{6}	7.0×10^{2}	1.8×10^{-4}
PLP2mut	5.0×10^{7}	6.0×10^{7}	1.2×10^{0}
MACmut	1.3×10^{7}	2.3×10^{5}	1.8×10^{-2}
MAC/PLP2mut	4.0×10^{6}	2.6×10^{2}	0.7×10^{-4}

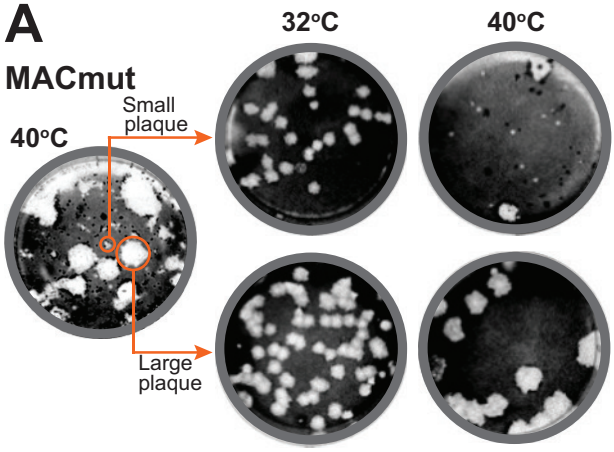

Representative isolate	Titer (PFU/mL) 32°C	40°C	EOP
Small plaque	1.3×10^{7}	2.3×10^{5}	1.8×10^{-2}
Large plaque	5.0×10^{7}	2.0×10^{7}	0.4×10^{0}